Inorganic Chemistry

pubs.acs.org/IC Article

Halogen-Bonded Cocrystals for Tunable Phosphorescence Emission of Pt Complexes

Mar I. García,[‖] Sergi Burguera,[‖] Ariadna Lázaro, Andrea Pinto, Jas S. Ward, Kari Rissanen, Laura Rodríguez,* and Antonio Frontera*

Cite This: https://doi.org/10.1021/acs.inorgchem.5c00372 Read Online

ACCESS | Metrics & More | Article Recommendations | Supporting Information

ABSTRACT: Noncovalent interactions, such as halogen bonding (HaB) and π-stacking, play a pivotal role in directing supramolecular assemblies and tuning photophysical properties. Herein, we report the synthesis, X-ray structural characterization, and photophysical properties of cocrystals and host:guest adducts formed by iodopentafluorobenzene (**G**) with three distinct Pt(II) complexes (**1**−**3**). The cocrystals exhibit a combination of short I···Pt halogen bonds and π-hole···Pt interactions in the solid state, highlighting the dual role of the Pt(II) center as a halogen bond acceptor and a π-stacking participant. Interestingly, an enhancement in emission intensity is observed for complexes **1**·**G** and **2**·**G** upon mixing of **1** or **2** with **G** in a chloroform solution, attributed to synergistic σ-hole···[d_z2-Pt^{II}] interactions that reduce the flexibility of the square-planar complex and the double heavy atom effect. These results emphasize the potential of host:guest interactions as a strategy for enhancing luminescence efficiency and open new avenues for designing functional materials for sensing and optoelectronic applications.

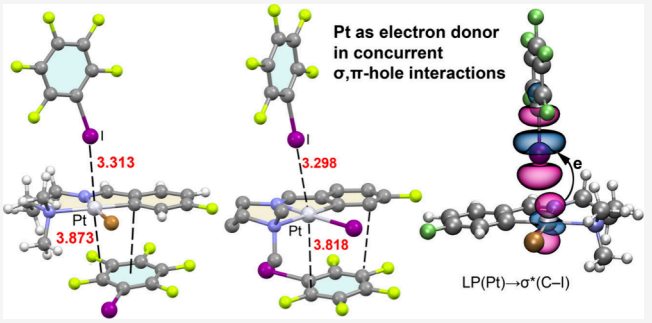

INTRODUCTION

Noncovalent interactions,[1−4] such as halogen bonding (HaB)[5] and chalcogen bonding (ChB),[6] have gained recognition as powerful tools in crystal engineering, facilitating the rational design of supramolecular architectures and functional materials. Halogen bonds, defined by IUPAC as net attractive interactions between an electron-deficient region (σ-hole) on a halogen atom and a nucleophilic region, are particularly notable for their high directionality and tunable strength.[7] The use of halogenated organic molecules, especially those containing iodine atoms, has proven instrumental in assembling supramolecular systems, where σ-hole interactions allow precise control over molecular organization.[5]

Typically, halogen bond acceptors are lone pair (LP) donor molecules such as amines, phosphines, amides, and oxoanions.[5] The incorporation of transition metal centers, such as Pt(II) and Pd(II), expands the repertoire of electron donors, introducing new interaction and structural possibilities.[8,9] Square-planar d^8-metal complexes, characterized by their nucleophilic d_z2 orbitals, can act as unconventional acceptors for σ-holes, forming halogen bonds with strengths comparable to those of hydrogen bonds and metal···metal interactions.[10] Moreover, the ability of these metal centers to simultaneously engage in σ-hole and π-hole interactions has opened exciting avenues for designing multifunctional materials.

Previous studies have emphasized the potential of combining σ-hole···[d_z2-Pt^{II}][11] and π-hole···[d_z2-Pt^{II}][12] interactions to construct robust supramolecular networks. The synergistic effects of these interactions have been exemplified in systems involving perfluorinated iodoarenes. For instance, platinum(II) complexes with dithiocarbamate ligands have been shown to form reverse sandwich structures through π-hole···[d_z2-M] stacking interactions,[13] highlighting the structural and functional importance of π-hole interactions in inorganic−organic systems.[14]

The ability of halogen bonding and iodinated species to act as dual σ-hole and π-hole donors has been shown to profoundly influence the assembly and photophysical properties of their cocrystals.[15,16] The electron-withdrawing nature of perfluorinated iodinated arenes enhances their electrophilicity, facilitating strong σ-hole interactions with metal centers and promoting π-stacking interactions with adjacent aromatic systems. These unique features have been effectively utilized in applications such as photoluminescent materials, catalysts, and sensors.

In this study, we present the synthesis and X-ray characterization of cocrystals formed by iodopentafluoroben-

Received: January 23, 2025
Revised: May 6, 2025
Accepted: May 12, 2025

https://doi.org/10.1021/acs.inorgchem.5c00372
Inorg. Chem. XXXX, XXX, XXX−XXX

zene (**G**) with three distinct Pt(II) complexes (**1**−**3**, see Scheme 1). Compounds **1** and **2** have a halogen heavy atom in

Scheme 1. Reaction of Pt(II) Cyclometalated Complexes with the Iodopentafluorobenzene Compound

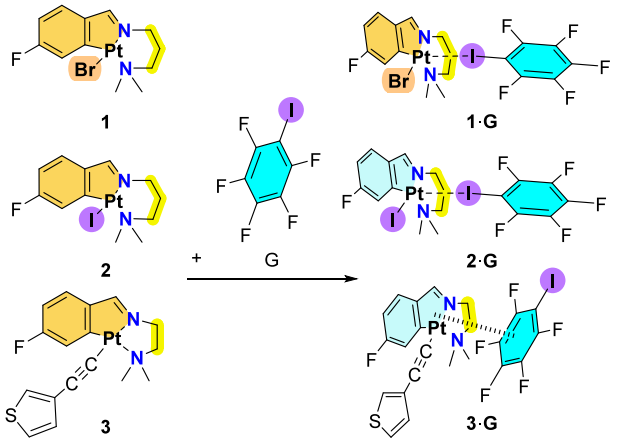

the coordination sphere of the Pt(II) center, while in compound **3**, this position is occupied by a more innocent ligand. Since we had already studied the emission properties of these three compounds, we saw them as ideal candidates to explore how the presence of a halogen heavy atom might influence molecular packing and introduce new weak interactions in cocrystals formed with a halogenated aromatic molecule. As a result, two of these cocrystals (derived from **1** and **2**) exhibit short Pt···I contacts, characteristic of halogen bonds, while all three display prominent [d_z2-Pt^{II}]···π-hole interactions in the solid state. These results highlight the cooperative roles of σ-hole and π-hole interactions in directing supramolecular assembly. Furthermore, the involvement of the platinum center in these noncovalent interactions underscores its dual role as a halogen bond acceptor and π-hole acceptor, driven by the nucleophilic dz^2 orbital (see Chart 1).

Chart 1. Coformers Used in This Work[a]

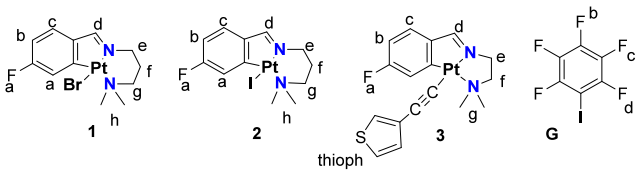

[a]Numbering of the positions has been included in this scheme with reference to the Experimental Section proton and fluorine assignment.

Furthermore, the photophysical behavior of the Pt(II) complexes reveals an enhancement in emission intensity upon mixing with iodopentafluorobenzene in solution. This luminescent behavior, attributed to changes in intermolecular interactions and electronic environments, demonstrates the potential of these systems for applications in sensing and optoelectronics. By integrating synthetic, structural, and photophysical investigations, this study highlights the interplay of halogen bonding and π-stacking interactions in shaping the structural and functional properties of metal−organic assemblies.

RESULTS AND DISCUSSION

Synthesis. The reaction of **1**−**3** with **G** leads to the formation of two type of new Pt(II) structures. While pentacoordinated square pyramidal Pt(II) complexes were accomplished by the reaction of **1** and **2** and the iodopentafluorobenze guest, π−π stacked adducts were formed in the case of **3** (Scheme 1).

The slow precipitation of the crystalline solid enabled the determination of its X-ray crystal structure, which also provided insights into the resulting optical properties (see below).

Structural Description. The structure of **1·G** (Figure 1) comprises two crystallographically independent molecules of

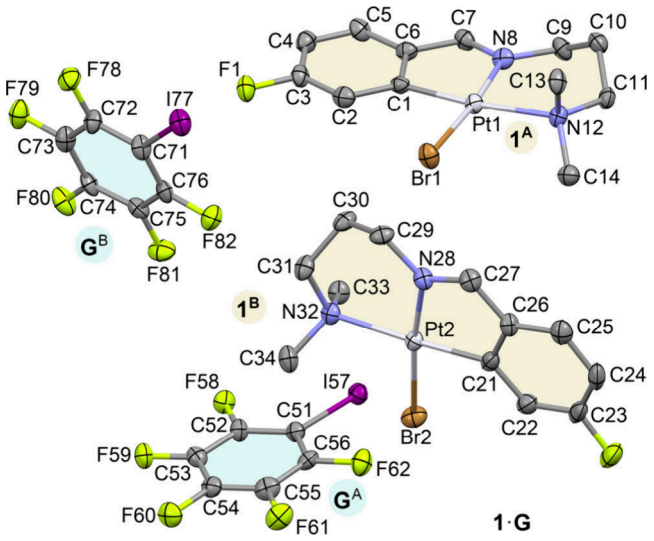

Figure 1. ORTEP representation of the asymmetric unit of compound **1·G**. Hydrogen atoms omitted for clarity; thermal ellipsoids at 50% probability level.

the platinum complex (designated as $\mathbf{1}^{A}$ and $\mathbf{1}^{B}$) and two distinct σ,π-hole donor molecules of C_6F_5I (designated as $\mathbf{G}^{A}$ and $\mathbf{G}^{B}$). The structural characteristics of the Pt(II) units closely resemble those observed in the XRD structure of the parent complex **1**, particularly in terms of planarity and coordination distances.[17] The preservation of bond lengths suggests that the electronic structure of the platinum complex remains largely unaffected by the cocrystal formation with **G**, emphasizing the delicate balance between molecular geometry and crystal packing forces.

In the **1·G** cocrystal (Figure 2), the platinum complex $\mathbf{1}^{A}$ interacts with $\mathbf{G}^{B}$ through an I77···F1 halogen bond [HaB: I··· F: 3.197(6) and ∠C−I···F: 176.8(3)°] and with $\mathbf{G}^{A}$ via π-stacking (inter centroid distance: 3.67 Å). Additionally, $\mathbf{1}^{B}$ interacts with the adjacent $\mathbf{G}^{B}$ molecule through a bifurcated C−H31,H33···F hydrogen bond. Furthermore, $\mathbf{1}^{B}$ establishes additional interactions, including a short I57···Pt2 halogen bond with $\mathbf{G}^{A}$ and π−π stacking with $\mathbf{G}^{B}$, which involves both the aromatic and Pt-chelate rings of the $\mathbf{1}^{B}$ unit (Figure 2b).

The asymmetric unit of **2·G** is simpler than that of **1·G**, comprising only one crystallographically independent molecule of the platinum complex and one of **G** (Figure 3a). It is worth noting that molecule **G** exhibits disorder in the cocrystal, as detailed in the ESI. For structural descriptions and theoretical calculations (*vide infra*), only the major component (87%) was considered.

https://doi.org/10.1021/acs.inorgchem.5c00372
Inorg. Chem. XXXX, XXX, XXX−XXX

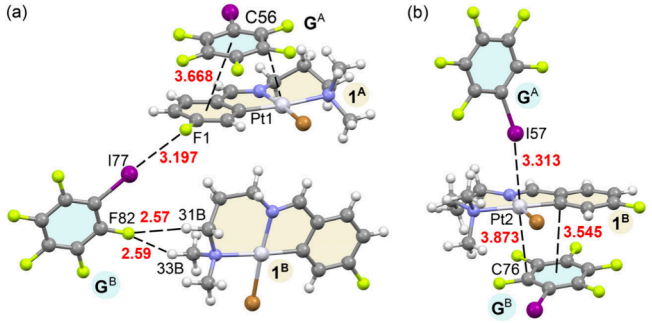

Figure 2. (a) Noncovalent interactions between $\mathbf{1}^{A}$, $\mathbf{1}^{B}$ and two **G** molecules. (b) Noncovalent interactions between $\mathbf{1}^{B}$ and two **G** molecules. Distances in Å.

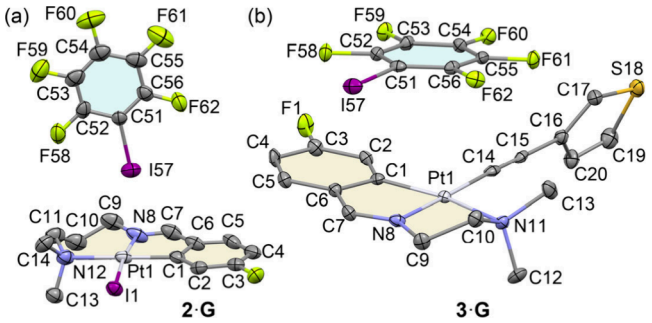

Figure 3. ORTEP representation of the asymmetric unit of compounds **2·G** (a) and **3·G** (b). Hydrogen atoms omitted for clarity; thermal ellipsoids at 50% probability level.

Similarly, the asymmetric unit of **3·G** (Figure 3b) consists of one platinum complex and one **G** molecule. The thiofuran ring in **3** displays disorder between two orientations, as described in the ESI, with only the major component (84%) depicted in Figure 3b and used for the DFT analysis below.

The supramolecular motif of cocrystal **2·G** (Figure 4a) is similar to that of $\mathbf{1}^{B}$**·G**, with each platinum complex

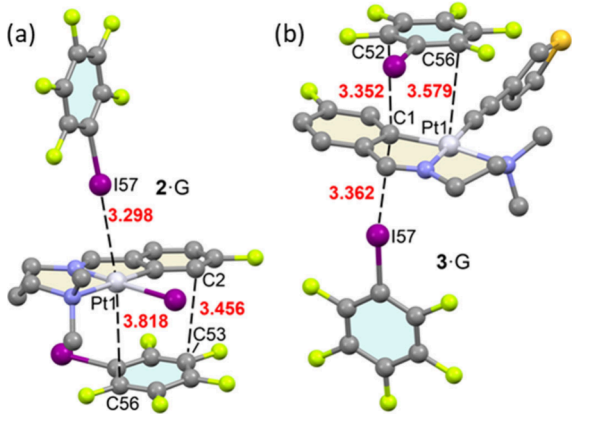

Figure 4. (a) Noncovalent interactions between **2** and two G molecules. (b) Noncovalent interactions between **3** and two G molecules. Distances in Å.

surrounded by two G molecules. One **G** molecule forms a directional I57···Pt1 halogen bond (HaB) with a slightly shorter distance (3.298(1) Å) compared to $\mathbf{1}^{B}$**·G**^{A}. The other G molecule engages in π-stacking, involving both the fluorophenyl group and the planar five-membered chelate ring.

In the cocrystal **3·G**, the platinum complex is again π-stacked with the **G** molecule on one side of the square planar Pt center, resembling the motifs observed in the **1·G** and **2·G** cocrystals, highlighting the recurrence of this supramolecular arrangement. A distinguishing feature of **3·G** is the absence of I···Pt halogen bond contacts. Instead, the G molecule forms an I57··· C1 HaB contact at a distance of 3.362(8) Å, which is shorter than the sum of Alvarez's[18] van der Waals radii, $\Sigma R_{vdW}(I + C)$ = 3.83 Å.

This structural analysis underscores the propensity of Pt to participate in noncovalent interactions, including metal-involving halogen bonds (HaBs), such as the I···Pt contacts identified in **1·G** and **2·G** (Figures 2b and 4a). These interactions were classified as HaBs based on a comprehensive evaluation of their geometric parameters, summarized in Table 1. Furthermore, all structures exhibit a partial π-hole···{dz^2-Pt(II)} interaction between the electron-deficient ring of **G** and the platinum metal center (Table 1, Figures 2 and 4). Notably, in the cocrystals of **1·G** and **2·G**, the Pt···C distances are significantly longer than in the **3·G** cocrystal, yet still shorter than the sum of van der Waals radii, $\Sigma R_{vdW}(Pt + C)$ = 4.06 Å (see Table 1). These findings illustrate the critical role of metal centers in noncovalent interactions, providing valuable insights into their structural and functional importance.

Table 1. Parameters of Selected Intermolecular Contacts in the Structures of Cocrystals (1−3)·G

Contact	Distance	Angle	Remark
1·G			
I57···Pt2	3.3131(7)	C51−I57···Pt2: 156.5(3)	σ-hole···[d_z2-Pt^{II}]
C56···Pt1	3.82(1)		π-hole···[d_z2-Pt^{II}]
C78···Pt2	3.87(1)		π-hole···[d_z2-Pt^{II}]
2·G			
I57···Pt1	3.298(1)	C51−I57···Pt1: 160.5(3)	σ-hole···[d_z2-Pt^{II}]
C56···Pt1	3.82(1)		π-hole···[d_z2-Pt^{II}]
3·G			
C56···Pt1	3.579(7)		π-hole···[d_z2-Pt^{II}]

It is important to emphasize that in all three structures, the metal-involving contacts are supported by additional noncovalent interactions (NCIs). The platinum(II) centers exhibit their ability to act as NCI acceptors, interacting with the σ-hole donating iodine atom in $\mathbf{1}^{B}$**·G**^{A} and **2·G**, while in all three cocrystals the arene π-hole engages with the d-orbital of the Pt(II) center. Notably, metal-involving halogen bonds (HaBs) of the type I···Pt are not unprecedented. Similar interactions have been reported in the literature for cocrystals containing bis-dialkylcyanamide halides, acetylacetonate, and dithiocarbamate platinum complexes with iodoperfluoroarenes.[8−10,14] Additionally, interactions between electron-deficient arene-based π-holes and the [d_z2-Pt^{II}] orbital have been well-documented across various systems.[12,13] These previous studies provide valuable context for our findings, underscoring that the I···Pt HaBs and π-hole···[d_z2-Pt^{II}] interactions observed in the cocrystals described herein are part of a broader phenomenon within iodine−platinum supramolecular chemistry.

Theoretical Considerations. This theoretical study focuses primarily on the σ,π-hole···[d_z2-Pt^{II}] interactions described in the preceding section, with particular emphasis on: (i) the I57···Pt2 and I57···Pt2 σ-hole interactions in the **1·G** and **2·G** compounds, respectively; and (ii) the C56···Pt1 π-

https://doi.org/10.1021/acs.inorgchem.5c00372
Inorg. Chem. XXXX, XXX, XXX−XXX

hole interactions observed in the three cocrystals reported in this work. Notably, fully optimized geometries were employed for all calculations.

Initially, we calculated the molecular electrostatic potential (MEP) surfaces for the **1**−**3** Pt complexes and the halogen bond donor molecule **G**, as shown in Figure 5, to identify the

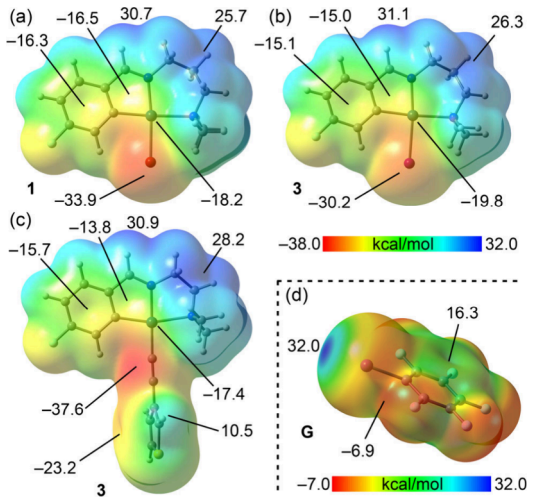

Figure 5. MEP surfaces of **1** (a), **2** (c), **3** (b) and **G** (d) at the RI-PBE0-D4/def2-TZVP. For compounds **1**−**3** the same energy scale was used. Isovalue 0.001 au.

most nucleophilic and electrophilic regions of the coformers utilized in this study. The MEP analysis revealed negative values at the Pt atom in all compounds, highlighting its nucleophilic character due to the filled d_z2-orbital. Additionally, the minimum MEP values were observed at the halide ligand in complexes **1** and **2** (−33.9 and −30.2 kcal/mol, respectively) and at the triple bond in complex **3** (−37.6 kcal/mol). The analysis also revealed significantly negative MEP values over the center of the C_6 ring of the ligand and the planar five-membered Pt-chelate ring, ranging from −13.8 to −16.5 kcal/mol. This indicates the presence of an extended π-basic surface, characterized by negative MEP values, which spans from the phenyl group through the fused five-membered chelate ring to the halide or ethynyl ligand. In all complexes, the maximum MEP value is observed in the region influenced by the imino hydrogen atom and the alkyl chain connecting the Pt-coordinated nitrogen atoms, with values close to 31 kcal/mol. Regarding the halogen bond donor molecule **G** (Figure 5d), the maximum MEP value is located at the iodine's σ-hole (32.0 kcal/mol), while the minimum is found at the fluorine atoms (−6.9 kcal/mol). The MEP value at the π-hole of **G** is 16.3 kcal/mol, which is notably lower than the value at the σ-hole.

To explore the relative ability of Pt complexes **1**−**3** to form dimers stabilized either by I···d_z2[Pt] halogen bonds (HBs) or π-stacking interactions, optimizations of (**1**−**3**)·**G** dimers were carried out at the RI-PBE0-D4/def2-TZVP level of theory. For compounds **1**·G and **2**·G, the study initially focused on the I···d_z2[Pt] dimers. The calculations confirm that both dimers are stable (true minima), indicating that their formation in the solid state is not merely a result of packing effects. Supporting this conclusion, the theoretical I···Pt distances were determined to be 3.16 Å, similar to those observed in the X-ray structures (see Table 1). Furthermore, the ∠C−I···Pt angles obtained from DFT calculations are 174.1° and 168.8° for **1**·**G** and **2**·**G**, respectively, which are in reasonable agreement with experimental values (156.5(3)° and 160.5(3)°, see Table 1). The theoretical distances are slightly shorter, and the angles are marginally larger than the experimental data, likely due to the absence of packing effects in the isolated dimers.

The optimized geometries, dimerization energies, and QTAIM/NCIPlot analyses of the I···d_z2[Pt] dimers in **1**·**G** and **2**·**G** are shown in Figure 6. The QTAIM analysis identifies

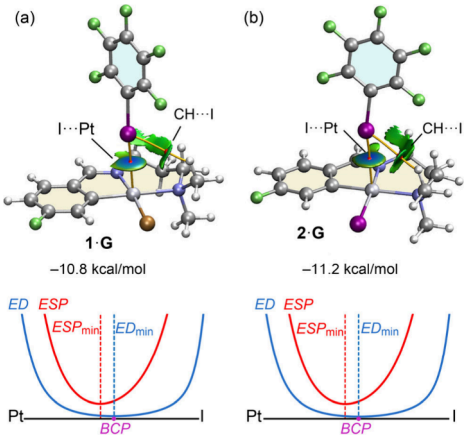

Figure 6. Top: Combined QTAIM (BCPs in red and bond paths as orange lines) and NCIplot analysis for the HaB dimer of compound **1**·**G** (a) and **2**·**G** (b). ED vs ESP plots for the I···Pt bond path of compound **1**·**G** (a) and **2**·**G** (b).

a bond critical point (BCP, depicted as a red sphere) and a bond path (depicted as an orange line) connecting the Pt and I atoms, confirming the presence of the I···Pt interaction. Additionally, the QTAIM analysis reveals the formation of an ancillary CH···I interaction involving a hydrogen atom of the alkyl chain. Both interactions are further characterized by reduced density gradient (RDG) isosurfaces: a blue, disk-shaped RDG isosurface for the I···Pt contact, indicating its strong nature, and green-colored RDG isosurfaces for the CH···I interactions, reflecting their weaker nature.

The binding energies of the dimers are moderately strong (−10.8 and −11.2 kcal/mol for **1**·**G** and **2**·**G**, respectively), underscoring the importance of these interactions. To confirm the halogen bond nature of the I···Pt contacts and rule out the possibility of coordination or semicoordination bonding, the electron density (ED) and electrostatic potential (ESP) along the bond path connecting the atoms were analyzed. In donor−acceptor interactions, the minimum electron density at the BCP is typically shifted toward the electron acceptor atom, while the ESP minimum is shifted toward the electron donor. In the I···dz^2[Pt] dimers, the ESP minimum is closer to the Pt atom (shown as a dashed red line in Figure 6, bottom), and the ED minimum (dashed blue line) is closer to the I atom, confirming the halogen bonding nature of the I···Pt interaction.

To further confirm the halogen bonding nature of the I··· d_z2[Pt] contacts (σ-hole interactions), we analyzed their donor−acceptor character using natural bond orbital (NBO) analysis, a valuable tool for examining charge transfer effects from an orbital perspective. The NBOs, shown in Figure 7, illustrate electron donation from the lone pair in the d_z2[Pt] orbital to the antibonding σ^*(I−C) orbital in both dimers. The corresponding stabilization energies are $E^{(2)}$ = 7.6 kcal/mol for **1**·**G** and $E^{(2)}$ = 6.9 kcal/mol for **2**·**G**, confirming the σ-hole

https://doi.org/10.1021/acs.inorgchem.5c00372
Inorg. Chem. XXXX, XXX, XXX−XXX

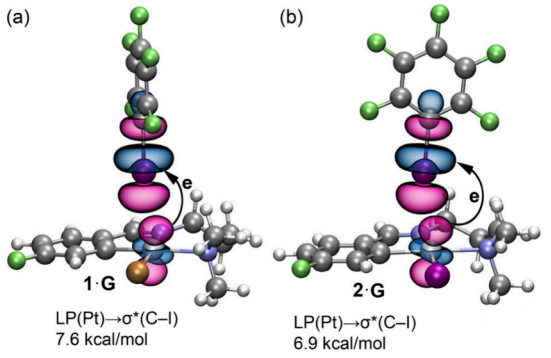

Figure 7. NBOs involved in the $d_z2[Pt] \rightarrow \sigma^*(I-C)$ and electron donation of the HaB dimers of **1·G** (a) and **2·G** (b).

interaction and highlighting the significant role of orbital effects in these complexes. Moreover, the second-order perturbation stabilization energy $E^{(2)}$ is higher in complex **1·G** than in **2·G**, which aligns with the greater directionality of the interaction (∠C–I···Pt = 174.1° and 168.8°, respectively). However, this is likely compensated by the stronger electrostatic attraction in **2·G**, as indicated by the larger MEP value at the Pt atom (see Figure 5), resulting in comparable overall interaction energies for both complexes (see Figure 6).

The QTAIM/NCIPlot analysis of the π-stacked dimers observed in the solid-state structures of compounds (**1**–**3**)**·G** is presented in Figure 7, alongside their interaction energies. The fully optimized dimers exhibit Pt···C distances that are slightly shorter than the experimental values, ranging from 3.52 to 3.57 Å. The QTAIM/NCIPlot analysis reveals large green reduced density gradient (RDG) isosurfaces between the arene rings of the ligands and the extended planes formed by the aromatic and fused chelate rings, indicating significant π-stacking interactions. Additionally, several bond critical points (BCPs) and bond paths are observed, linking the perfluoroiodobenzene and the metallacyclic rings, as well as aliphatic H-atoms from the methyl and methylene groups. A distinctive feature across all dimers is the linkage of the Pt atom to a carbon atom of G, underscoring the metal's active role in the binding mechanism.

The binding energies for the π-stacked dimers are higher than those of the σ-hole dimers (Figure 6), primarily due to the combined contribution of π-stacking and CH···F contacts. This explains the predominant formation of such adducts in the solid-state structures of all compounds. While there is little variation in the binding energies of the π-stacked dimers across the three cocrystals, the dimer in **3·G** is slightly stronger (−15.2 kcal/mol). This can be attributed to the additional thiophene ring in compound **3**, which facilitates the formation of an extra CF···H contact, as confirmed by the QTAIM and NCIPlot analysis (see Figure 8c).

Correlation between Host:Guest Cocrystallization Products and Emission Properties. The interaction between the guest molecule and complexes **1**–**3** in dichloromethane solution was investigated using absorption and emission spectroscopy. The results reveal that the interaction of **G** with complexes **1** and **2** is remarkably strong, with similar features with the bromide and iodide platinum host compound. Significant changes in the emission spectra are observed even upon the initial addition of the guest molecule, when a complete 1:1 adduct is not yet expected to form (Figure 9 and S1). These spectral changes are attributed to the

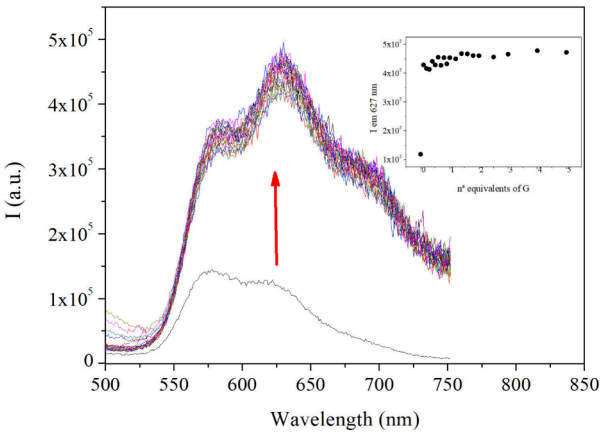

Figure 9. Emission spectra of **1** at room temperature in $1 \cdot 10^{-4}$ M dichloromethane solution upon addition of increasing amounts of **G** (left). λ_{exc} = 385 nm (air-equilibrated solutions).

formation of noncovalent σ-hole···$[d_z2\text{-}Pt^{II}]$··· and π-hole··· $[d_z2\text{-}Pt^{II}]$ interactions, which modify the shape of the emission spectrum. Notably, a pronounced increase in emission intensity is recorded, further highlighting the impact of these interactions.

The observed increase in emission intensity can be attributed to the double heavy atom effect, which enhances spin–orbit coupling and results in more efficient phosphorescence and they agree with the platinum complexes origin according to their excitation spectra (see SI). Square planar Pt(II) complexes typically exhibit strong metal–ligand bonding and efficient spin–orbit coupling, leading to characteristic phosphorescence in the visible range. This increased flexibility reduces spin–orbit coupling efficiency, potentially lowering emission intensity or altering the emission profile.[19] The interaction of iodide, a heavy atom, with the Pt(II) center reinforces spin–orbit coupling and reduces the flexibility, thereby increasing emission intensity and shifting the emission spectrum. Emission quantum yields and lifetimes were measured for complexes **1**–**3** and the corresponding

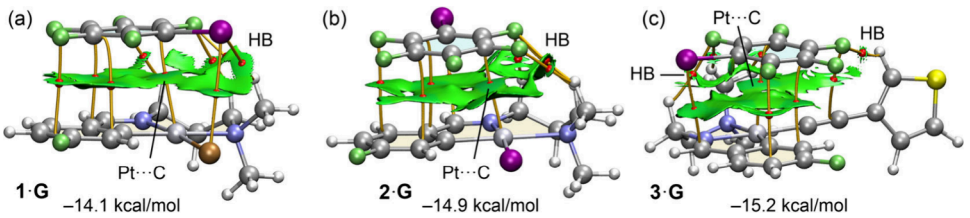

Figure 8. Combined QTAIM (BCPs in red and bond paths as orange lines) and NCIplot analysis for the π-stacking heterodimer of compound **1·G** (a), **2·G** (b) and **3·G** (c).

https://doi.org/10.1021/acs.inorgchem.5c00372
Inorg. Chem. XXXX, XXX, XXX–XXX

host:guest **1**−**3**·**G** adducts (Table 2) in order to get insight into these experimental observations.

Table 2. Emission Quantum Yields (QY), Lifetimes (τ), and Corresponding Calculated Radiative (k_r) and Nonradiative (k_{nr}) Rate Constants for the Compounds and Corresponding Host:Guest Adducts in Air Equilibrated Solutions

Compound	QY	τ (ns)	k_r (s^{-1})	k_{nr} (s^{-1})
1	0.004	147	2.72×10^{04}	6.78×10^{06}
2	0.005	157	3.18×10^{04}	6.34×10^{06}
3	0.009	211	4.27×10^{04}	4.70×10^{06}
1·G	0.04	156	2.56×10^{05}	6.15×10^{06}
2·G	0.02	186	1.08×10^{05}	5.27×10^{06}
3·G	0.01	168	5.95×10^{04}	5.89×10^{06}

As can be seen in Table 2, the emission quantum yields of compounds **1** and **2** increase one order of magnitud upon the formation of the corresponding **1·G** and **2·G** adducts while only a slight increase of this value is recorded in the case of **3**. This is, obviously, compatible with the observations of the increase on the emission intensity in these two cases. The calculation of the radiative and nonradiative rate constants allow us to observe that the formation of the adducts are mainly affecting the radiative rate constants, supporting our previous statement based on the double heavy atom effect, that favors the intersystem crossing causing a more efficient emissive process in the case of **1·G** and **2·G**.

No significant changes have been observed in the corresponding absorption and ^{1}H NMR spectra titration data (Figures S3−S8). This can indicate that the different modes of interaction with **G** are mainly affecting the excited states. The corresponding emission data in the solid state would be crucial for comparing the X-ray crystallographic information with the photophysical properties. Unfortunately, neither the Pt(II) precursors[17,19] nor the resulting adducts exhibit emission in the solid state, making such a direct comparison unfeasible. Nevertheless, the emission changes observed in solution are still highly relevant. These changes clearly affect both the emission profiles and the radiative and nonradiative rate constants in the presence of the guest molecule, supporting the role of the double heavy atom effect in modulating the emissive properties of the compounds.

It is noteworthy that prior studies have demonstrated that π-hole···[d_z2-Pt^{II}] interactions with electron-deficient arenes enhance the phosphorescence of Pt(II)-based luminophores, with the extent of enhancement being proportional to the size of the electron-deficient arene and the strength of the π-hole··· [d_z2-Pt^{II}] interaction. However, in the current study, emission enhancement is observed only for complexes **1·G** and **2·G**. Interestingly, compound **3·G** (Figure S2), which lacks σ-hole··· [d_z2-Pt^{II}] interactions in the solid state, exhibits only a slight increase in emission intensity compared to the isolated Pt(II) complex **3**. Instead, a broader emission band is observed, which can be attributed to the π-stacked arrangement of the **3·G** adduct, as seen in its solid-state structure. These findings suggest that the enhancement of emission intensity is primarily due to σ-hole···[d_z2-Pt^{II}] interactions rather than π-hole···[d_z2-Pt^{II}] interactions. The latter are present exclusively in the solid-state structures of **1·G** and **2·G**. The results also reinforce the significance of the double heavy atom effect mechanism.

These observations underscore the potential of host:guest interactions as a strategy for enhancing emission efficiency, a feature that has been explored only sparingly in the literature. This approach offers a promising avenue for designing luminophores with improved photophysical properties for advanced applications.

CONCLUSIONS

In this study, we demonstrated the critical role of noncovalent interactions, specifically σ-hole···[d_z2-Pt^{II}] and π-hole···[d_z2-Pt^{II}] interactions, in the formation and photophysical behavior of adducts formed by iodopentafluorobenzene (**G**) and three distinct Pt(II) complexes (**1**−**3**). The structural analysis revealed that the Pt(II) center acts as both a halogen bond acceptor and a π-stacking participant, embracing π-hole···[d_z2-Pt^{II}] contacts, stabilizing the supramolecular assemblies. Notably, an enhancement in phosphorescence emission was observed for complexes **1·G** and **2·G**, attributed to the synergistic effects of σ-hole interactions and the double heavy atom effect, which facilitates increased spin−orbit coupling. In contrast, complex **3·G**, which lacks σ-hole interactions, exhibited only a slight emission enhancement with a broader spectral band due to its π-stacked arrangement. In depth photophysical analysis indicates that the enhancement on the emission properties of **1·G** and **2·G** are mainly due to a clear increase (1 order of magnitude) on the radiative rate constants in the presence of **G**. These findings underscore the potential of host:guest interactions as a powerful strategy for modulating the photophysical properties of Pt(II)-based materials, offering valuable insights for the design of advanced luminophores with applications in sensing and optoelectronics.

EXPERIMENTAL SECTION

General Procedures. Commercial reagent iodopentafluorobenzene was purchased from Merck. Compounds **1**−**3** were prepared by previously reported procedures.[17,19]

Crystal Data. The single crystal X-ray data for **1·G**, **2·G** and **3·G** were collected at 120 K using an Agilent SuperNova diffractometer fitted with a HyPix-Arc 100 detector using mirror-monochromated Cu−Kα (λ = 1.54184 Å) radiation. All structures were solved by intrinsic phasing (SHELXT)[20] and refined by full-matrix least-squares on F^2 using Olex2,[21] utilizing the SHELXL module.[22] Anisotropic displacement parameters were assigned to non-H atoms and isotropic displacement parameters for all H atoms were constrained to multiples of the equivalent displacement parameters of their parent atoms with U_{iso}(H) = 1.2 U_{eq}(CH, CH_2) or 1.5 U_{eq}(CH_3) of their respective parent atoms. The X-ray single crystal data and CCDC numbers of all new structures are included in the Supporting Information.

Physical Measurements. Infrared spectra have been recorded on a Fourier transform infrared (FT-IR) 5700 Nicolet Spectrophotometer. The elemental analyses of all compounds were performed at the Serveis Científics i Tecnològics of the Universitat de Barcelona using a Carlo Erba model EA1108 elemental analyzer. ^{1}H NMR (δ(TMS) = 0.0 ppm) spectra have been obtained on a Bruker 400. ^{19}F(δ(TMS) = 0.0 ppm) spectra have been obtained on a Bruker 500. Absorption spectra have been recorded on a Varian Cary 100 Bio UV spectrophotometer, and emission spectra have been recorded on a Horiba Jobin-Yvon SPEX Nanolog spectrofluorimeter.

Theoretical Calculations. The full geometry optimizations, without imposing symmetry constraints, and energetic calculations were carried out using the Turbomole 7.7 software package[23] at the PBE0-D4/def2-TZVP level of theory.[24−27] Molecular electrostatic potential (MEP) surfaces were generated using an isosurface value of 0.001 au. The magnitude and sign of the potential V(r) are the same as would be the interaction energy of the system with a unit positive

https://doi.org/10.1021/acs.inorgchem.5c00372
Inorg. Chem. XXXX, XXX, XXX−XXX

point charge (a proton). It is customary to express V(r) in units of energy rather than energy/charge, as corresponds to a potential. Thus, energies reported here are in kcal/mol. The quantum theory of atoms in molecules (QTAIM)[28] and noncovalent interaction plot (NCIPlot)[29] analyses were performed at the same computational level and visualized with the VMD software.[30] The Multiwfn program[31] was utilized for QTAIM and NCIPlot calculations, while natural bond orbital (NBO) analysis[32] was conducted using the NBO7 program.[33]

Synthesis and Characterization. *Synthesis of [PtBr{$(CH_3)_2N(CH_2)_3NCH(4\text{-}FC_6H_3)$}$(C_6F_5I)$] (**1·G**).* 400 μL of 3 mM dichloromethane solution of [PtBr{$(CH_3)_2N(CH_2)_3NCH(4\text{-}FC_6H_3)$}] was made react with 400 μL of 3 mM solution of C_6F_5I and the solution was kept under stirring for 1 min at room temperature. Single crystals precipitate after 2 weeks from the solution media upon slow diffusion of hexane into the dichloromethane solution. The resolution of the crystalline samples by single crystal X-ray diffraction verified the formation of the desired adduct. ^{1}H NMR ($CDCl_3$, 400 MHz): δ 8.33 [t,1H, ^4J(H−H) = 1.5, ^3J(Pt−H) = 143.7, H^d]; 8.00 [dd, 1H, ^3J(F−H) = 10.7, ^4J(H−H) = 2.5, ^3J(Pt−H) = 46.6, H^a]; 7.26 [m, 1H, H^c]; 6.68 [td, 1H, ^3J(F−H) = ^3J(H−H) = 8.5, ^4J(H−H) = 2.5, H^b]; 3.86 [t, 2H, ^3J(H−H) = 5.1, ^3J(Pt−H) = 35.2, H^e]; 2.86 [m, 8H, H^{g,h}]; 2.03 [qi, 2H, ^3J(H−H) = 5.6, H^f]. ^{19}F NMR ($CDCl_3$, 500 MHz): δ −103.81 [m, 1F^a], −118.89 [dd, 2F^c], −151.82 [t, F^b], −159.09 [td, 2F^d]. IR: ν 1604.89 (C = C) Anal. Found (calcd. for $C_{18}H_{16}BrF_6IN_2Pt$): C 27.32 (27.85); H 2.06 (2.08); N 3.58 (3.61).

*Synthesis of [PtI{$(CH_3)_2N(CH_2)_3NCH(4\text{-}FC_6H_3)$}$(C_6F_5I)$] (**2·G**).* Similar experimental procedure was performed for the synthesis of **2** but using [PtI{$(CH_3)_2N(CH_2)_3NCH(4\text{-}FC_6H_3)$}] as platinum source. ^{1}H NMR ($CDCl_3$, 400 MHz): δ 8.45 [dd,1H, ^3J(F−H) = 11.4, 4J(H−H) = 2.5, ^3J(Pt−H) = 38.9, H^a]; 8.38 [t, 1H, ^4J(H−H) = 1.7, ^3J(Pt−H) = 135.8, H^d]; 7.26 [m, 1H, H^c]; 6.65 [td, 1H, ^3J(F−H) = ^3J(H−H) = 8.4, ^4J(H−H) = 2.6, H^b]; 3.83 [t, 2H, ^3J(H−H) = 5.6, H^e]; 3.01 [s, 6H, ^3J(Pt−H) = 16.7, H^h]; 2.81 [m, 2H, H^g]; 2.05 [qi, 2H, ^3J(H−H) = 5.7, H^f]. ^{19}F NMR ($CDCl_3$, 500 MHz): δ −103.71 [m, 1F^a], −118.90 [dd, 2F^c], −151.88 [t, 1F^b], −159.08 [td, 2F^d]. IR: ν 1599.02 (C = C). Anal. Found (calcd. for $C_{18}H_{16}F_6I_2N_2Pt$): C 26.19 (26.26); H 1.99 (1.96); N 3.43 (3.40).

*Synthesis of [Pt(C≡Cthiophene){$(CH_3)_2N(CH_2)_2NCH(4\text{-}FC_6H_3)$}$(C_6F_5I)$] (**3·G**).* Similar experimental procedure was performed for the synthesis of **3** but using [Pt(C≡Cthiophene){$(CH_3)_2N(CH_2)_2NCH(4\text{-}FC_6H_3)$}] as platinum source. ^{1}H NMR ($CDCl_3$, 400 MHz): δ 8.35 [s,1H, ^3J(Pt−H) = 80.9, H^d], 7.56 [dd, 1H, ^3J(F−H) = 9.6, ^4J(H−H) = 2.7, ^3J(Pt−H) = 70.7, H^a]; 7.24 [m, 2H, H^{c,tioph}]; 7.19 [dd, 1H, ^3J(H−H) = 4.9, ^3J(H−H) = 3.0, H^{thioph}], 7.14 [dd, 1H, ^3J(H−H) = 4.9, ^3J(H−H) = 1.1, H^{thioph}], 6.66 [td, 1H, ^3J(F−H) = ^3J(H−H) = 8.6, ^4J(H−H) = 2.5, H^b], 4.03 [t, 2H, ^3J(H−H) = 6.4, H^e], 3.14 [t, 2H, ^3J(H−H) = 6.0, H^f], 3.04 [s,6H, ^3J(Pt−H) = 20.5, H^g]. ^{19}F NMR (CDCl3, 500 MHz): δ −103.64 [s, 1F^a], −118.93 [dd, 2F^c], −151.88 [t, 1F^b], −159.11 [td, 2F^d]. IR: ν 2106.19 (C≡C). Anal. Found (calcd. for $C_{25}H_{23}F_6IN_2PtS$): C 36.66 (36.64); H 2.80 (2.83); N 3.38 (3.42); S 3.86 (3.91).

Spectrophotometric and Spectrofluorimetric Titrations. Titrations were carried out at 25 °C in air-equilibrated dichloromethane by the addition of aliquots of 1 × 10^{-2} M solution of of C_6F_5I to a 1 × 10^{-4} M solution of compound the Pt(II) complex. until reaching 5 equiv. Absorption and emission spectra were recorded after each addition.

■ ASSOCIATED CONTENT

Supporting Information

The Supporting Information is available free of charge at https://pubs.acs.org/doi/10.1021/acs.inorgchem.5c00372.

Additional details on the characterization data including NMR, X-ray crystallography, and photophysical data; computational data (PDF)

Accession Codes

Deposition Numbers 2418518−2418520 contain the supplementary crystallographic data for this paper. These data can be obtained free of charge via the joint Cambridge Crystallographic Data Centre (CCDC) and Fachinformationszentrum Karlsruhe Access Structures service.

■ AUTHOR INFORMATION

Corresponding Authors

Laura Rodríguez − *Departament de Química Inorgànica i Orgànica, Secció de Química Inorgànica,, Universitat de Barcelona, and Institut de Nanociència i Nanotecnologia (IN2UB), 08028 Barcelona, Spain;* orcid.org/0000-0003-1289-1587; Email: laurarodriguezr@ub.edu

Antonio Frontera − *Departament de Química, Universitat de les Illes Balears, 07122 Palma de Mallorca (Baleares), Spain;* orcid.org/0000-0001-7840-2139; Email: toni.frontera@uib.es

Authors

Mar I. García − *Departament de Química Inorgànica i Orgànica, Secció de Química Inorgànica,, Universitat de Barcelona, and Institut de Nanociència i Nanotecnologia (IN2UB), 08028 Barcelona, Spain*

Sergi Burguera − *Departament de Química, Universitat de les Illes Balears, 07122 Palma de Mallorca (Baleares), Spain*

Ariadna Lázaro − *Departament de Química Inorgànica i Orgànica, Secció de Química Inorgànica,, Universitat de Barcelona, and Institut de Nanociència i Nanotecnologia (IN2UB), 08028 Barcelona, Spain*

Andrea Pinto − *Departament de Química Inorgànica i Orgànica, Secció de Química Inorgànica,, Universitat de Barcelona, and Institut de Nanociència i Nanotecnologia (IN2UB), 08028 Barcelona, Spain;* orcid.org/0000-0001-9491-7140

Jas S. Ward − *Department of Chemistry, University of Jyvaskyla, 40014 Jyväskylä, Finland;* orcid.org/0000-0001-9089-9643

Kari Rissanen − *Department of Chemistry, University of Jyvaskyla, 40014 Jyväskylä, Finland;* orcid.org/0000-0002-7282-8419

Complete contact information is available at: https://pubs.acs.org/10.1021/acs.inorgchem.5c00372

Author Contributions

‖M.I.G. and S.B. contributed equally to this work.

Notes

The authors declare no competing financial interest.

■ ACKNOWLEDGMENTS

The authors are grateful for Projects PID2020-115637GB-I00, PID2022-139296NB-I00, and PID2023-148453NB-I00 funded by the Ministerio de Ciencia, Innovación y Universidades of Spain MCIU/AEI/10.13039/501100011033 and FEDER, UE. This article is based upon work from COST Action CA22131, LUCES Supramolecular LUminescent Chemosensors for Environmental Security, supported by COST (European Cooperation in Science and Technology).

■ REFERENCES

(1) Jena, S.; Dutta, J.; Tulsiyan, K. D.; Sahu, A. K.; Choudhury, S. S.; Biswal, H. S. Noncovalent interactions in proteins and nucleic acids:

beyond hydrogen bonding and π-stacking. *Chem. Soc. Rev.* **2022**, *51*, 4261−4286.
(2) Haque, Ashanul; Alenezi, Khalaf M.; Khan, Muhammad S.; Wong, Wai-Yeung; Raithby, Paul R. *Chem. Soc. Rev.* **2023**, *52*, 454−472.
(3) Alkorta, I.; Elguero, J.; Frontera, A. Not Only Hydrogen Bonds: Other Noncovalent Interactions. *Crystals* **2020**, *10*, 180.
(4) Schneider, H.-J. Noncovalent interactions: A brief account of a long history. *J. Phys. Org. Chem.* **2022**, *35*, No. e4340.
(5) Cavallo, G.; Metrangolo, P.; Milani, R.; Pilati, T.; Priimagi, A.; Resnati, G.; Terraneo, G. The Halogen Bond. *Chem. Rev.* **2016**, *116*, 2478−2601.
(6) Mahmudov, K. T.; Gurbanov, A. V.; Aliyeva, V. A.; Guedes da silva, M. F. C.; Resnati, G.; Pombeiro, A. J. L. Chalcogen bonding in coordination chemistry. *Coord. Chem. Rev.* **2022**, *464*, 214556.
(7) Desiraju, G. R.; Ho, P. S.; Kloo, L.; Legon, A. C.; Marquardt, R.; Metrangolo, P.; Politzer, P.; Resnati, G.; Rissanen, K. Definition of Halogen Bonding (IUPAC Recommendations 2013). *Pure Appl. Chem.* **2013**, *85*, 1711−1713.
(8) Rozhkov, A. V.; Ivanov, D. M.; Novikov, A. S.; Ananyev, I. V.; Bokach, N. A.; Kukushkin, V. Y. Metal-involving halogen bond Ar−I···[dz2PtII] in a platinum acetylacetonate complex. *CrystEngComm* **2020**, *22*, 554−563.
(9) Zelenkov, L. E.; Eliseeva, A. A.; Baykov, S. V.; Suslonov, V. V.; Galmés, B.; Frontera, A.; Kukushkin, V. Y.; Ivanov, D. M.; Bokach, N. A. Electron belt-to-σ-hole switch of noncovalently bound iodine(i) atoms in dithiocarbamate metal complexes. *Inorg. Chem. Front* **2021**, *8*, 2505−2517.
(10) Benito, I.; Gomila, R. M.; Frontera, A. On the energetic stability of halogen bonds involving metals: implications in crystal engineering. *CrystEngComm* **2022**, *24*, 4440−4446.
(11) Rozhkov, A. V.; Katlenok, E. A.; Zhmykhova, M. V.; Ivanov, A. Y.; Kuznetsov, M. L.; Bokach, N. A.; Kukushkin, V. Y. Metal-Involving Chalcogen Bond. The Case of Platinum(II) Interaction with Se/Te-Based σ-Hole Donors. *J. Am. Chem. Soc.* **2021**, *143*, 15701−15710.
(12) Katlenok, E. A.; Kuznetsov, M. L.; Cherkasov, A. V.; Kryukov, D. M.; Bokach, N. A.; Kukushkin, V. Y. Metal-involved C···dz2-PtII tetrel bonding as a principal component of the stacking interaction between arenes and the platinum(ii) square-plane. *Inorg. Chem. Front.* **2023**, *10*, 3916−3928.
(13) Blasi, D.; Nicolai, V.; Gomila, R. M.; Mercandelli, P.; Frontera, A.; Carlucci, L. Unprecedented $\{dz^2\text{-}CuIIO_4\}\cdots\pi$-Hole Interactions: The Case of a Cocrystal of a Cu(II) Bis-β-Diketonate Complex with 1,4-Diiodotetrafluorobenzene. *Chem. Commun.* **2022**, *58* (69), 9524−9527.
(14) Ivanov, D. M.; Bokach, N. A.; Kukushkin, V. Y.; Frontera, A. Metal Centers as Nucleophiles: Oxymoron of Halogen Bond-Involving Crystal Engineering. *Chem.—Eur. J.* **2022**, *28*, No. e202103173.
(15) Wang, W.; Zhang, Y.; Jin, W. J. Halogen bonding in room-temperature phosphorescent materials. *Coord. Chem. Rev.* **2020**, *404*, 213107.
(16) Rozhkov, A. V.; Ananyev, I. V.; Gomila, R. M.; Frontera, A.; Kukushkin, V. Y. π-Hole···dz^2[PtII] Interactions with Electron-Deficient Arenes Enhance the Phosphorescence of PtII-Based Luminophores. *Inorg. Chem.* **2020**, *59*, 9308−9314.
(17) Lázaro, A.; Serra, O.; Rodríguez, L.; Crespo, M.; Font-Bardia, M. Luminescence studies of new [C,N,N0] cyclometallated platinum-(II) and platinum(IV) compounds. *New J. Chem.* **2019**, *43*, 1247−1256.
(18) Alvarez, S. A cartography of the van der Waals territories. *Dalton Trans.* **2013**, *42*, 8617−8636.
(19) Lazaro, A.; Cunha, C.; Bosque, R.; Pina, J.; Ward, J. S.; Truong, K.-N.; Rissanen, K.; Lima, J. C.; Crespo, M.; Seixas de Melo, J. S.; Rodríguez, L. Room-Temperature Phosphorescence and Efficient Singlet Oxygen Production by Cyclometalated Pt(II) Complexes with Aromatic Alkynyl Ligands. *Inorg. Chem.* **2020**, *59*, 8220−8230.
(20) Sheldrick, G. M. SHELXT - Integrated Space-Group and Crystal-Structure Determination. *Acta Crystallogr. Sect. A Found. Crystallogr.* **2015**, *71*, 3−8.
(21) Dolomanov, O. V.; Bourhis, L. J.; Gildea, R. J.; Howard, J. A. K.; Puschmann, H. OLEX2: A Complete Structure Solution, Refinement and Analysis Program. *J. Appl. Crystallogr.* **2009**, *42*, 339−341.
(22) Sheldrick, G. M. Crystal Structure Refinement with SHELXL. *Acta Crystallogr. Sect. C Struct. Chem.* **2015**, *71*, 3−8.
(23) Ahlrichs, R.; Bär, M.; Häser, M.; Horn, H.; Kölmel, C. Electronic structure calculations on workstation computers: The program system turbomole. *Chem. Phys. Lett.* **1989**, *162*, 165−169.
(24) Adamo, C.; Barone, V. Toward reliable density functional methods without adjustable parameters: The PBE0 model. *J. Chem. Phys.* **1999**, *110*, 6158−6170.
(25) Caldeweyher, E.; Ehlert, S.; Hansen, A.; Neugebauer, H.; Spicher, S.; Bannwarth, C.; Grimme, S. A generally applicable atomic-charge dependent London dispersion correction. *J. Chem. Phys.* **2019**, *150*, 154122.
(26) Weigend, F. Accurate Coulomb-fitting basis sets for H to Rn. *Phys. Chem. Chem. Phys.* **2006**, *8*, 1057−1065.
(27) Weigend, F.; Ahlrichs, R. Balanced basis sets of split valence, triple zeta valence and quadruple zeta valence quality for H to Rn: Design and assessment of accuracy. *Phys. Chem. Chem. Phys.* **2005**, *7*, 3297−3305.
(28) Bader, R. F. W. A quantum theory of molecular structure and its applications. *Chem. Rev.* **1991**, *91*, 893−928.
(29) Contreras-garcía, J.; Johnson, E. R.; Keinan, S.; Chaudret, R.; Piquemal, J.-P.; Beratan, D. N.; Yang, W. NCIPLOT: A Program for Plotting Noncovalent Interaction Regions. *J. Chem. Theory Comput.* **2011**, *7*, 625−632.
(30) Humphrey, W.; Dalke, A.; Schulten, K. VMD: Visual molecular dynamics. *J. Mol. Graphics* **1996**, *14*, 33−38.
(31) Lu, T.; Chen, F. Multiwfn: A multifunctional wavefunction analyzer. *J. Comput. Chem.* **2012**, *33*, 580−592.
(32) Glendening, E. D.; Landis, C. R.; Weinhold, F. Natural bond orbital methods. *WIREs Comput. Mol. Sci.* **2012**, *2*, 1−42.
(33) Glendening, E. D.; Badenhoop, J. K.; Reed, A. E.; Carpenter, J. E.; Bohmann, J. A.; Morales, C. M.; Karafiloglou, P.; Landis, C. R.; Weinhold, F. *NBO 7.0*; 2018.

https://doi.org/10.1021/acs.inorgchem.5c00372
Inorg. Chem. XXXX, XXX, XXX−XXX